Use of High-Resolution
Upwind Scheme for Vortical Flow Simulations*

Kozo FUJII** and Shigeru OBAYASHI***

ABSTRACT

For vortical flow simulations at high Reynolds numbers, it is important to keep the artificial dissipation as small as possible since it induces unphysical decay of the vortex strength. One way to accomplish this is to decrease the grid spacing. Another way is to use computational schemes having little dissipation. In the present paper, one of the high-resolution upwind schemes called 'MUSCL with Roe's average' is applied to vortical flow fields.

Two examples are considered. One is the leading-edge separation-vortex flow over a strake-delta wing. The other is a high-angle of attack supersonic flow over a spaceplane-like geometry. Comparison with the central difference solutions indicates that the present upwind scheme is less dissipative and thus has better resolution for the vortical flows.

概　　　要

高レイノルズ数の剥離渦流れの数値計算では，剥離渦の数値粘性による減衰をさけるために人工的な粘性効果をできるかぎりおさえる必要がある。格子の数を増やし離散化による誤差を減らすのは最も手っ取り早い方法であろう。もう1つの方法はより小さな人工粘性項をもつ計算手法を利用することである。我々の興味はベクトル的な未知量を持ったシステム方程式であるから，このことは直接に高次精度化を意味するものではない。別の言い方をすれば同じ次数であっても不要な人工粘性を避け，なおかつ安定な計算手法を構築することが可能である。ここでは最近広く利用されてきた高精度風上差分法－Roeの平均化を用いたMUSCL法を利用し，中心差分の場合の解と比較しその有効性を議論する。例としてはダブルデルタ翼上の亜音速剥離渦流れとスペースプレーンまわりの超音速剥離渦流れ：　りあげる。その結果，この手法は，非粘性の不連続や境界層について良い特性をもっているだけでなく剥離渦流れについても優れた特性を示すことが明らかとなった。

1. INTRODUCTION

The flow over aircraft and missiles at moderate to high angles of attack is characterized by the presence of large spiral vortices on the leeward side of the body. These separation vortices induce low pressure on the body upper surface, and this low pressure is the predominant factor of the resulting aerodynamic characteristic of the body. Research on such flow is of great importance practically as well as physically because understanding of the separated and vortical flow fields may lead to the control of vortex behavior and eventually to the enhancement of flight vehicle performance.

The rapid progress of supercomputers and numerical methods has made computer simulation of such vortical flows feasible. (Recent efforts in computational methods and application results were surveyed by Newsome and Kandil, see Ref. 1). Three-dimensional Reynolds-averaged Navier-Stokes equations used for various flow simulations have become a primary method for the vortical flow simulations since they can describe separated vortical flows with no special treatment. There exists one important fact that should be kept in mind. Typical computational grids used for Navier-Stokes simulations are fine only near the body surface to resolve viscous layers. These grid distributions are adequate for those flows where important phenomena only occur near the body surface as embedded shock waves or flow separation. For vortical flow simulations, on the other hand, not only the region near the body surface but also regions away from the body surface are important. Since the strength of vortices which are located away from the body is a dominant factor of the flow field, grid resolution away from the body is critical for an accurate simulation of vortical flow. Rai in Ref. 2 pointed out that conventional, spatially second-order accurate finite-difference schemes are much too dissipative for calculations involving vortices that travel large distances. Reference 3 studied the effect of grid resolution for vortical flow simulations and found the important result that vortex breakdown phenomenon cannot be predicted unless a sufficiently fine grid is used.

Now, how can we obtain accurate solutions for the vortical flows with computer memory and time constraints? High-order upwind differencing has become popular in recently-developed Euler methods for compressible inviscid flows. This feature has been extended in the straightforward manner for the evaluation of the convective terms of Navier-Stokes computations (see Refs. 4-6, for instance). Discontinuities are more sharply captured by these upwind methods com-

pared to those by conventional central difference method with additional numerical dissipation, since high-order upwind methods introduce minimum amount of dissipation needed to prevent oscillations. Recently, the matrix form of the dissipation terms implicitly introduced by upwind methods was studied[7)-9)] and it was shown that such terms in the upwind schemes such as Roe's flux difference splitting become small in the viscous layers. As artificial dissipation should be kept to a minimum and viscous effects near the body surface should be correctly evaluated in vortical flow simulations, high-resolution upwind method may be adequate for vortical flow simulations.

The object of the present work is to demonstrate the capability of high-resolution upwind method for accurate vortical flow simulations. Two flow fields are considered as application examples. One is a subsonic flow over a strake-delta wing. Simulation of the same flow fields was already conducted by the first author using a conventional central difference method. The same grid distributions: fine grid and medium grid are used for comparison. The second example is a supersonic flow over a spaceplane-like geometry. The flow field is much more complicated in this example since there exist bow shock wave, wing shock wave, fuselage vortex, strake vortex and wing vortex.

2. GOVERNING EQUATIONS AND NUMERICAL ALGORITHM

Compressible Navier-Stokes Equations

The basic equations under consideration are the unsteady Navier-Stokes equations written for a body-fitted coordinate system (ξ, η, ζ).

$$\partial_\tau \hat{Q} + \partial_\xi \hat{E} + \partial_\eta \hat{F} + \partial_\zeta \hat{G} = Re^{-1} \partial_\zeta \hat{S} \qquad (1)$$

In Eq. (1), the thin-layer approximation has been introduced. The use of thin-layer Navier-Stokes equations is justified because the viscous effects are confined to a thin layer near the wall and are dominated by the viscous terms associated with the strain rates normal to the wall,

and because the flow away from the body is essentially rotational inviscid. The contribution of the viscous terms in the shear layer rolling up from the surface wall and core of the vortices is assumed to be negligible. It should be noted that the viscous terms are not properly evaluated in these regions even by the full Navier-Stokes equations because of the grid deficiency.

The pressure, density, and velocity components are related to the energy for an ideal gas by

$$p = (\gamma - 1) \left[e - \rho \left(u^2 + v^2 + \omega^2 \right)/2 \right] \qquad (2)$$

LU-ADI Algorithm with Upwind Feature

The time-integration algorithm used here is the LU-ADI factorization method proposed by Obayashi et al. for two-dimensional problems. An extension to three-dimensional problems is described in Ref. 11. This algorithm decomposes the usual block tridiagonal system of Beam and Warming's into the product of lower and upper scalar bidiagonal matrices using a diagonal form and an approximate LDU decomposition. The basic algorithm is first-order accurate in time. In this original LU-ADI scheme, the convective terms are evaluated using second- or fourth-order central differencing and the viscous terms are evaluated using second-order central differencing in the right-hand side. Since the delta form is used, steady state solutions are indifferent to the left-hand-side operators, and depend only on the right-hand-side steady state description. Thus, steady state solutions can be improved by modifying the right-hand-side discretization method.

In the right-hand side, convective terms are now evaluated using flux difference splitting by Roe.[12] The MUSCL interpolation is used for the higher-order extension following Ref. 9. Central differencing that is adopted in the original LU-ADI code is used just for the comparison. In that case, nonlinear artificial dissipation terms are added (see Ref. 13), and their coefficients are set to be reasonable values that have been successfully used for many practical computations.

Higher-order extension of flux difference splitting using the MUSCL approach is found in Ref. 9, but is briefly described again. When the convective terms are differenced with the flux-difference splitting of Roe, the spatial derivatives are written in the conservative form as a flux balance. For instance in the ξ-direction,

$$\left(\frac{\partial \hat{F}}{\partial \xi} \right) = \left(\hat{F}_{j+1/2} - \hat{F}_{j-1/2} \right)/\left(\xi_{j+1/2} - \xi_{j-1/2} \right) \qquad (3)$$

The numerical flux $\hat{F}_{j+1/2}$ can be written as the solution to an approximate Rieman problem and the necessary metric terms are evaluated at the cell interface $j + 1/2$.

$$\hat{F}_{j+1/2} = \frac{1}{2} \left[\tilde{F}(Q_L) + \tilde{F}(Q_R) \right.$$
$$\left. - |\tilde{A}| (Q_R - Q_L) \right]_{j+1/2}, \qquad (4)$$

where $\tilde{F}$ is the flux vector and $\tilde{A}$ is the corresponding Jacobian matrix computed using Roe's average state $\tilde{}$. Q_L and Q_R are the state variables to the left and right of the half-cell interface. These state variables are determined from the locally one-dimensional non-oscillatory interpolations called MUSCL approach. Primitive variables q [ρ, u, v, w, P] are used for that purpose, and high-order accurate monotone differencing is given by a one-parameter κ.

$$(q_L)_{j+1/2} = q_j + \frac{s}{4} \left[(1 - \kappa s) \Delta_- + (1 + \kappa s) \Delta_+ \right]_j$$
$$(q_R)_{j+1/2} = q_{j+1} - \frac{s}{4} \left[(1 - \kappa s) \Delta_+ + (1 + \kappa s) \Delta_- \right]_{j+1}. \qquad (5)$$

where

$$(\Delta_+)_j = q_{j+1} - q_j, (\Delta_-)_j = q_j - q_{j-1}.$$
$$s = \frac{2 \Delta_+ \Delta_- + \epsilon}{(\Delta_+)^2 + (\Delta_-)^2 + \epsilon}$$

s is the Van Alabama limiter and κ is a small constant to prevent zero division. For all the results here, third-order accuracy corresponding to $\kappa = 1/3$ is used. Near the boundary, the MUSCL interpolation goes down to the first-order.

3. RESULTS

### Computed Results for Subsonic Flow over a Strake-Delta Wing

First example is the subsonic flow over a strake-delta wing. The flow field was extensively studied experimentally by Brennenstuhl and Hummel[14] in a low-speed wind tunnel and computationally by one of the present authors. The freestream Mach number is 0.3, and the Reynolds number based on the root chord is 1.3×10^6 in the following computations.

The angle of attack for the first case is 12 degrees. At this angle of attack, there exist two vortices over the upper surface of the wing; one emanating from the strake leading edge and the other from the main-wing leading edge. These two vortices merge together over the main-wing surface because of the mutual interaction. Figures 1a and 1b show the overall view of the spanwise total pressure contour plots at several chordwise stations. The result obtained by the upwind differencing is plotted in Fig. 1a, and the result by the central (with added dissipation) differencing is plotted in Fig. 1b. The total number of grid points is about 850,000; 119 points in the chordwise direction, 101 points circumferentially and 71 points in the normal direction. Details of the grid generation and the grid distribution can be found in Ref. 15. Both results indicate the existence of two vortices over the wing surface and their interaction. It seems that the merging of the two vortices is slightly delayed in the upwind solution. The corresponding particle path traces showing the vortex trajectories are shown in Fig. 2 for the upwind result. The comparison of the computed vortex trajectories with the experiment that was already done for the central differencing result in Ref. 15 is also presented in this figure. It is clear that merging of two vortices are delayed in the upwind result, but still earlier than the experiment at the same Reynolds number. For further comparison, the spanwise total pressure contour plots

(with twice the number of contours lines) and density contour plots as 65% chordwise location are depicted in Figs. 3a-4b. Figures 3a and 3b are the results obtained by the upwind differencing, and Figs. 4a and 4b are the results by the central differencing. Both contour plots show strong gradients due to the viscous layers near the surface. Upwind result shows that this region is thinner compared to the central differencing result. This may be reasonable since numerical dissipation introduced by the present upwinding is small in the viscous boundary layers as explained in Ref. 9.

The same computation was carried out using smaller number of grid points (called medium grid in Ref. 3, about 120,000 in total). Compared to the previous grid, the number of the grid points are decreased in all the directions. Figures 5a and 5b represent the total pressure contour plots obtained by the upwind and central difference computations, respectively. The upwind result shown in Fig. 5a indicates the existence of two vortices and their merging process although the inner vortex is not as distinct as the fine grid result. On the other hand, the central difference result in Fig. 5b shows only one flattened vortex instead of two vortices.

It is recognized from these results that the present upwind scheme has better resolution than the conventional central difference scheme on the same grid although grid resolution itself is, of course, an important factor for an accurate flow simulation. Upwind scheme is more "vortex-preserving" than central differencing scheme (with added dissipation) since it has a lower level of dissipation. In the present upwind scheme where the dissipation terms are constructed in the matrix form, each characteristic wave has its own minimum dissipation. On the other hand, central difference scheme where dissipation terms are constructed in the scalar form, requires amount of dissipation which is large enough for all the waves. This is the reason that the upwind
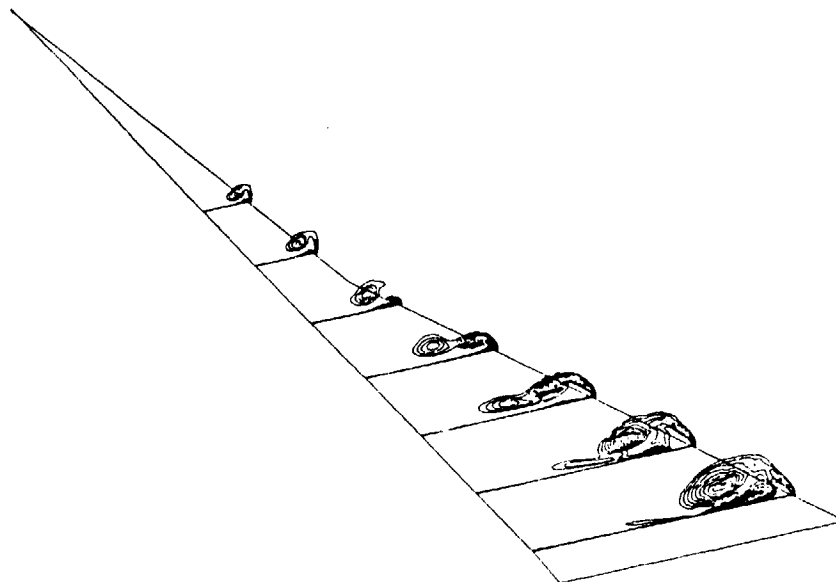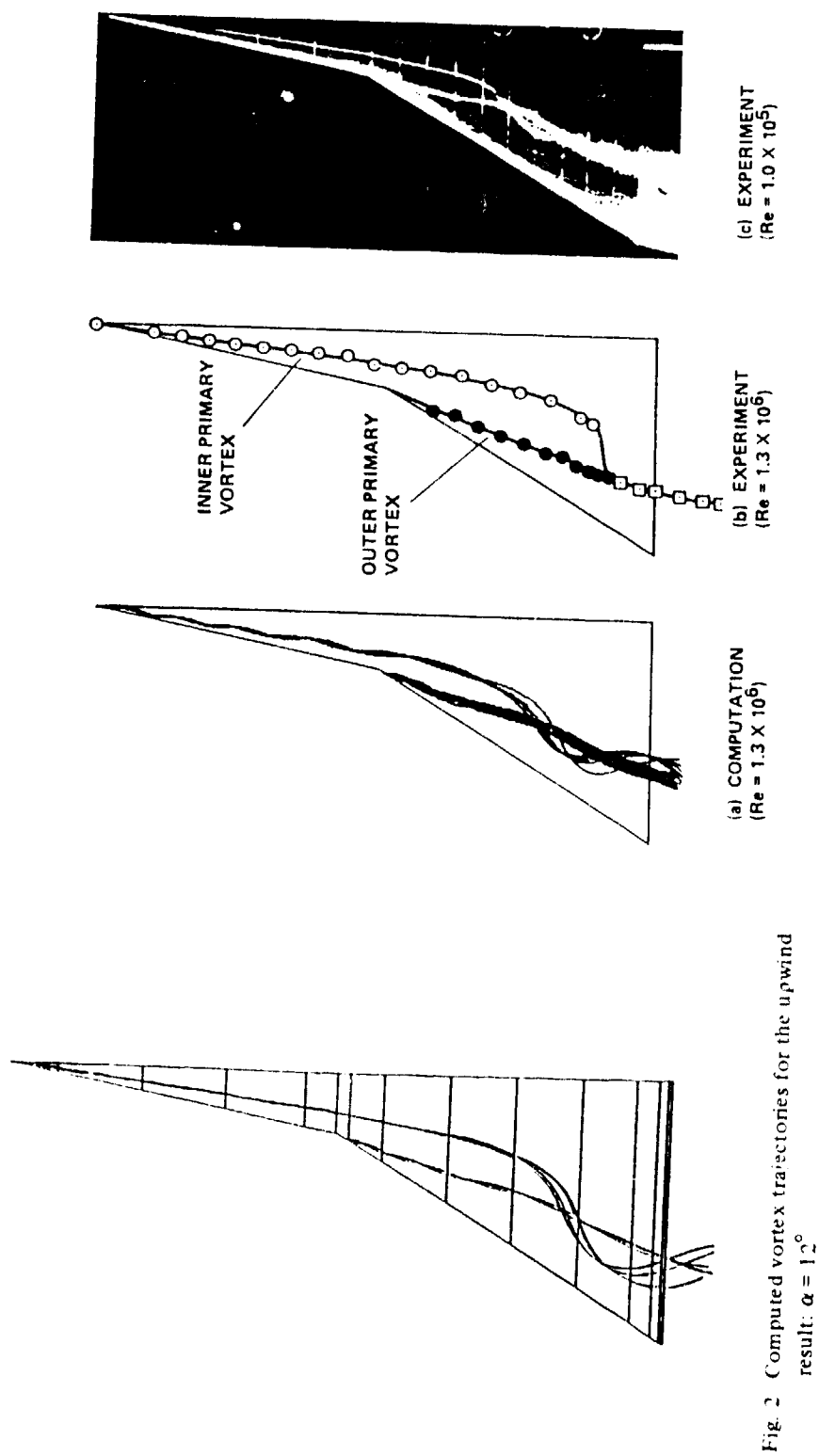
a) upwind difference result
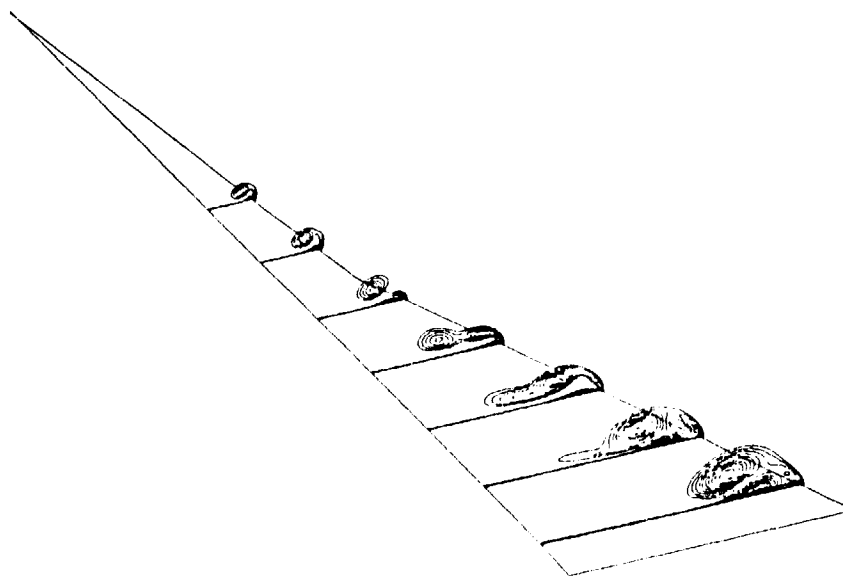
b) central difference result

Fig. 1 Spanwise total pressure contour plots: $\alpha = 12^\circ$
overall view of the fine grid solution –

(c) EXPERIMENT
(Re = 1.0 X 10⁵)

(b) EXPERIMENT
(Re = 1.3 X 10⁶)

INNER PRIMARY VORTEX

OUTER PRIMARY VORTEX

(a) COMPUTATION
(Re = 1.3 X 10⁶)

Fig. 2 Computed vortex trajectories for the upwind
result: $\alpha = 12°$

a) total pressure contour

b) density contour
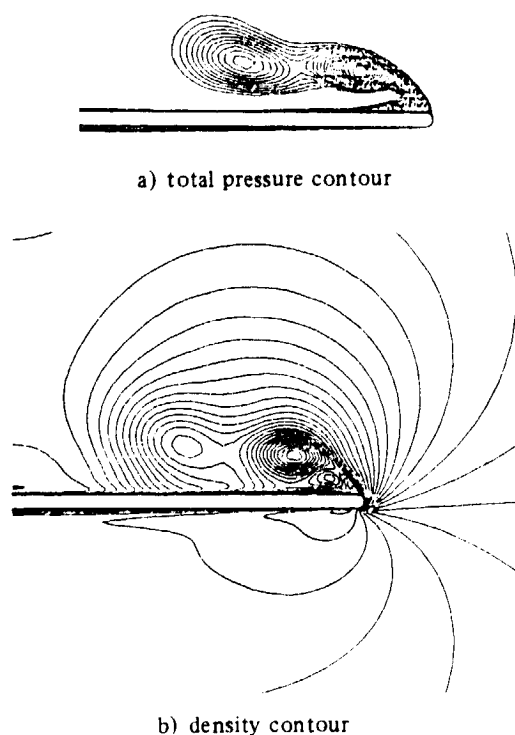
Fig. 3 Spanwise contour plots at 65% chord by the upwind scheme: $\alpha = 12°$

a) total pressure contour

b) density contour

Fig. 4 Spanwise contour plots at 65% chord by the central difference scheme: $\alpha = 12°$

scheme like the one used here is less dissipative and has better resolution.

Of course, solution of both central and upwind difference schemes should converge to the solution of the original partial differential equations as the computational grid is refined. The accuracy estimation based on the idea of the Tailor expansion is important but not good enough for the system of nonlinear equations. What we need in numerical schemes is the better representation of the properties of original partial differential equations and, in that sense, upwind difference scheme shows better result than that of the central difference scheme for the grid distributions feasible under the memory restriction of the current supercomputers.

The angle of attack for the second case is 30 degrees. Only the calculations for the medium grid (previously mentioned grid of about 120,000 points) computati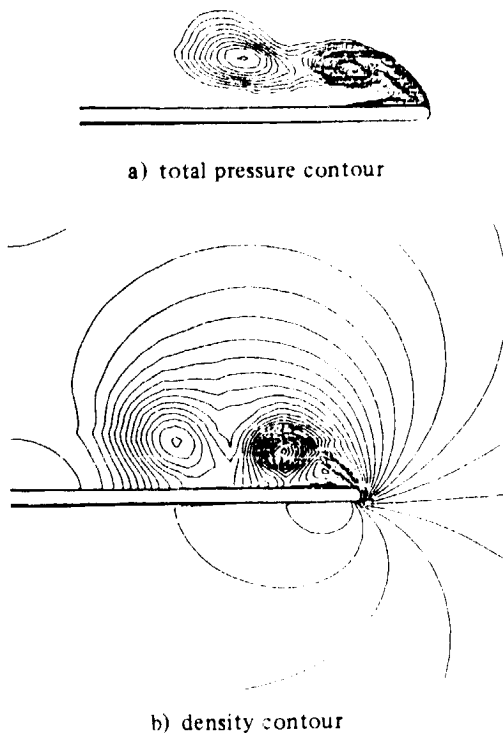on is carried out. At this angle of attack, both the experiment and the computational results using the fine grid showed that vortex breakdown takes place near the trailing edge. The computed total pressure contour plots are presented in Figs. 6a and 6b. An abrupt increase of the vortex-core is observed near the trailing edge in the upwind result shown in Fig. 5a. This indicates that the vortex has undergone breakdown. In fact, the plot of the streamwise velocity (although not shown here) showed that there exists the reverse flow region near the trailing edge. The central difference result shown in Fig. 6b, on the other hand, does not show such a sudden change. Again, the resolution is enhanced by the use of the present upwind scheme at least on the grid used here although a slight increase of the number of grid points may introduce breakdown phenomenon also in the central difference result.
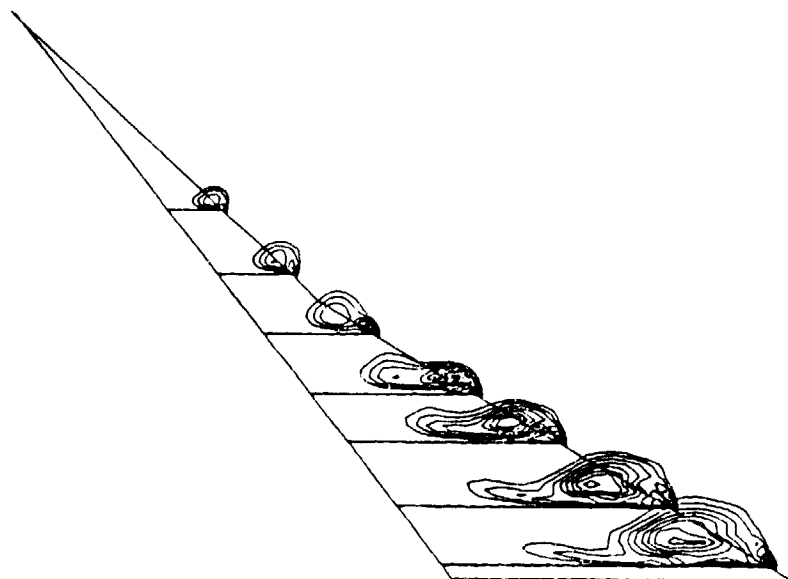
a) upwind result
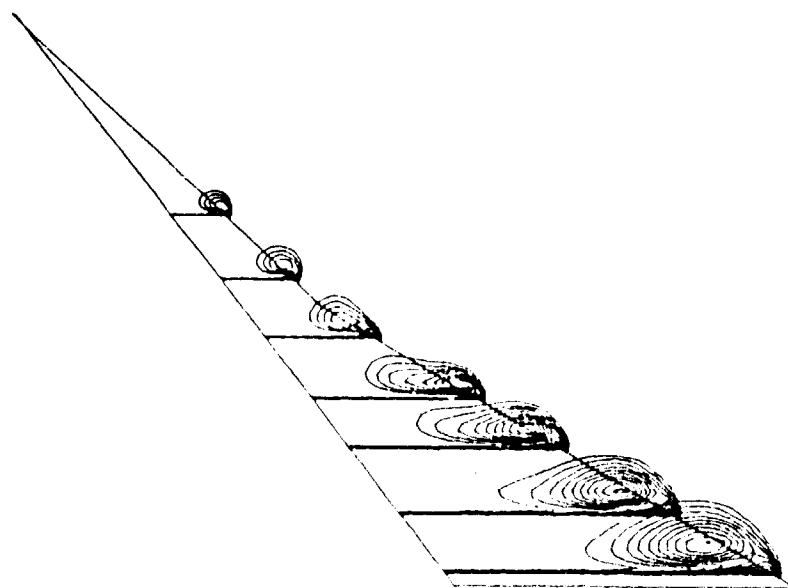
b) central difference result

Fig. 5 Computed total pressure contour plots: $\alpha = 12^\circ$
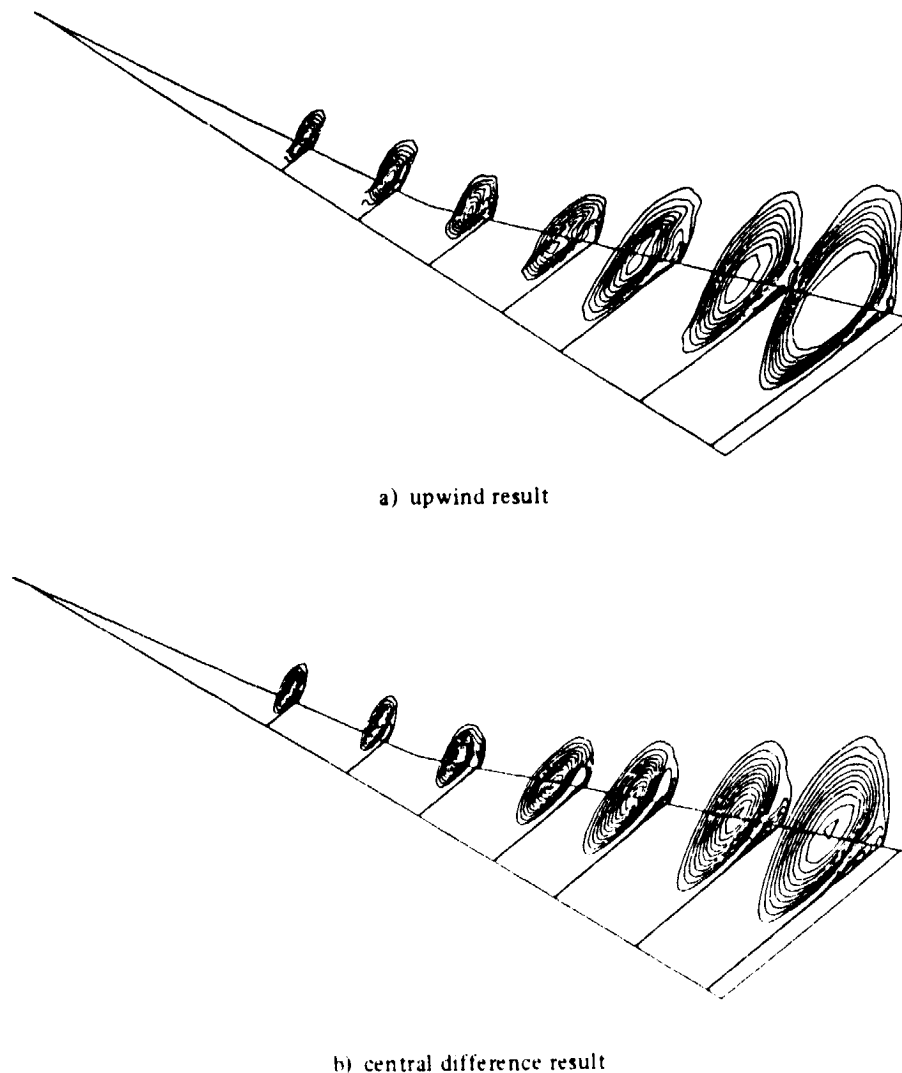overall view of the medium grid solution

a) upwind result

b) central difference result

Fig. 6 Computed total pressure contour plots: $\alpha = 30°$
overall view of lthe medium grid solution

Computed Results for Supersonic Flow over a Spaceplane

Computations were carried out at the Mach number, 1.5, the Reynolds number, 1.0×10^6 based on the maximum span length, and the angle of attack 20 degrees. The configuration has only fuselage and strake-wing corresponding to the experimental model. Figure 7 shows an overview of the surface grid over this geometry. Topologically, the grid is of C-type in the chord-wise direction and 0-type in the circumferential direction, and consists of 89 points in the chordwise direction, 103 points in the circumferential direction and 40 points from the body to the outer boundary. The minimum spacing near the body surface is carefully set to be 0 (10^{-5}) with the span length unity. The outer boundary is located outside of the bow shock which is captured. In the computation, bilateral symmetry is assumed and the half of the volume is
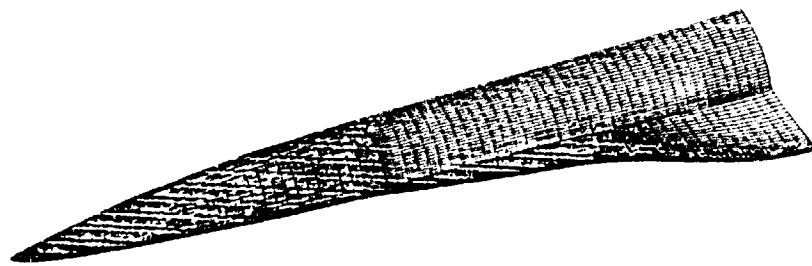
Fig. 7   Overall view of the computational grid for the spaceplane

solved. At the end of the body geometry, zero-th order extrapolation is applied as the outflow condition. Even for this simplified geometry, the flow field is complicated since there exist bow shock, strake and wing shocks and leading-edge separation vortices. Thus, it is important to use an accurate solution scheme both for linear waves and nonlinear waves. Figures 8a and 8b show the overall density contour plots for the upwind and central difference solutions, respectively. Since the present upwind scheme is TVD-type, all the shock waves; bow shock wave from the nose, wing shocks from the strake and the wing, are captured better in Fig. 8a compared to the central difference result shown in Fig. 8b. Streamwise periodic structure observed near the symmetry plane on the fuselage surface indicates the separation vortex from the fuselage is developed in the streamwise direction. It is noticed that contours over the surface especially near the wing-fuselage junction are significantly different between Figs. 8a and 8b. Also noticed is the kink of the contour lines on the fuselage surface where the strake begins. This may be due to the distribution of the grid and the effect is pronounced when the upwind differencing is used.

Two cross-sectional plots are presented to show the detail. Crossflow density plots at the forward fuselage section (= 16% chord) are shown in Fig. 9, with the upwind result presented on the left, and the central difference result on the right. Again, bow shock is clearer in the up-

wind result. The central difference solution demonstrates stronger primary vortex although both solutions produce the primary vortex. This may be caused by the artificial dissipation terms implemented in the central difference computation. In other words, central difference solution represents sort of relatively "lower Reynolds number flow" near the body surface because of the added dissipation and thus the flow tends to separate more easily. The cross-sectional geometry is composed of the flat region in the bottom and circular region on the top. At the junction, another separation may be recognized in the upwind solution although not clearly seen. Figure 10 shows the similar plots for the rear portion of the geometry (= 98% chord). One interesting feature here is the existence of the crossflow shock wave in the upwind solution. Experimental flow visualization for the crossflow was not carried out and thus it is impossible to say which solution is physically correct. However, it is important that different flow fields are obtained by the two different solution schemes.

4. CONCLUSION

For vortical flow simulations at high Reynolds number, it is important to keep artificial dissipation as small as possible since resolution is critical for an accurate simulation. One way is to decrease the truncation error by reducing the grid spacing. Numerical experiments shown in the present paper indicated that the present upwind scheme has better resolution on the same grid
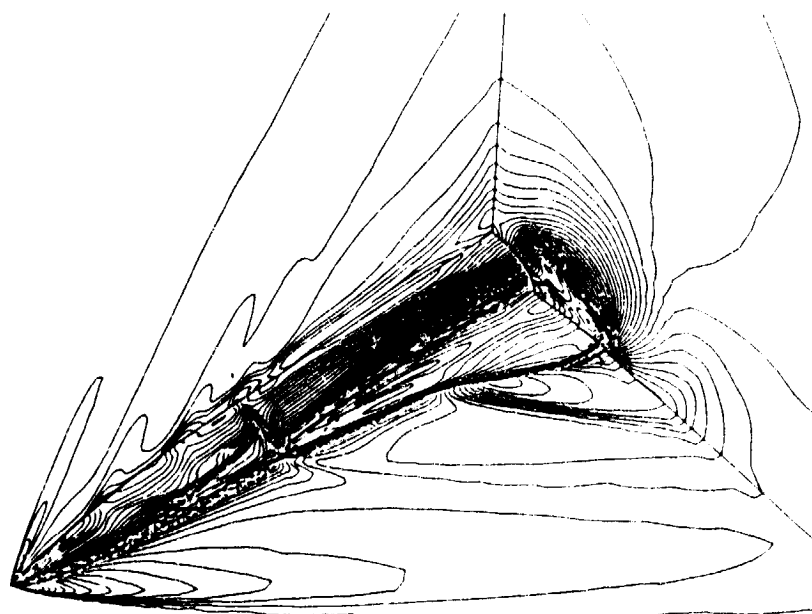
a) upwind result
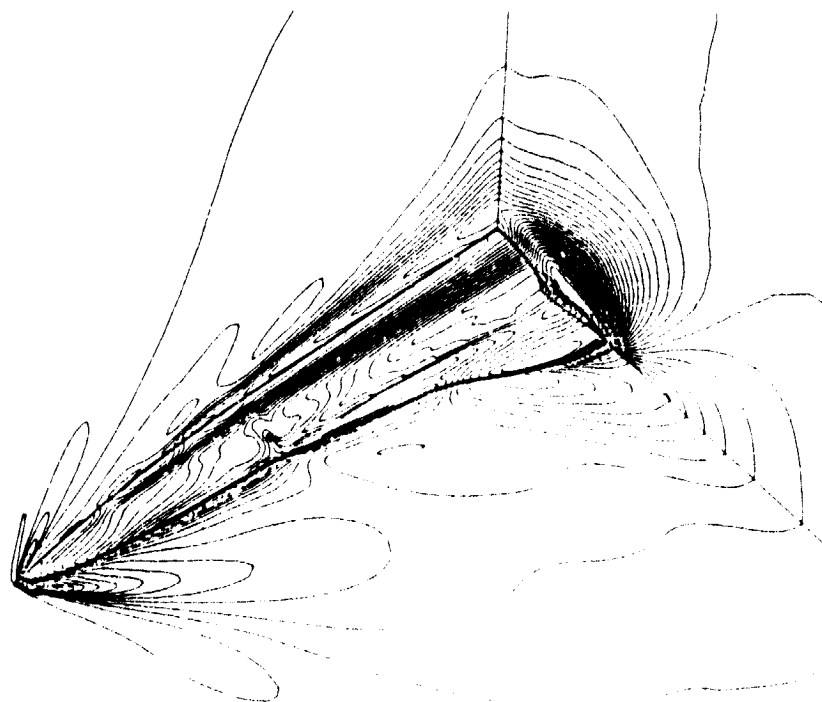
b) central difference result

Fig. 8 Overall view of the computed density contour plots over a spaceplane
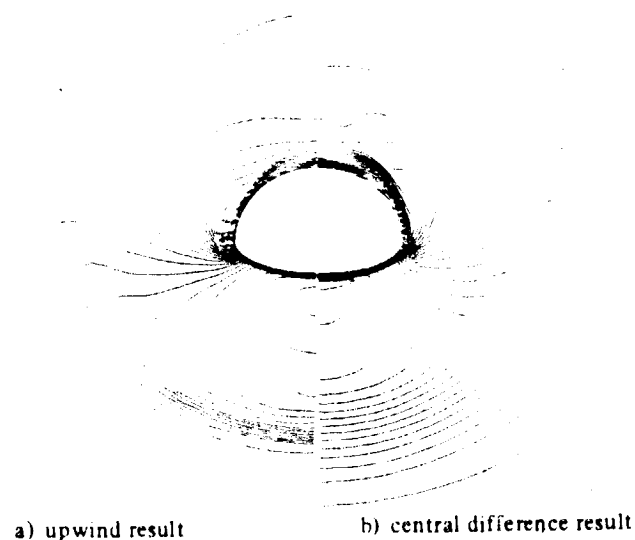$M_\infty = 1.5$, $\alpha = 20°$

a) upwind result   b) central difference result

Fig. 9   Spanwise plots of the computed density contours over a spaceplane
(x/c = 16%): $M_\infty = 1.5$, $\alpha = 20°$

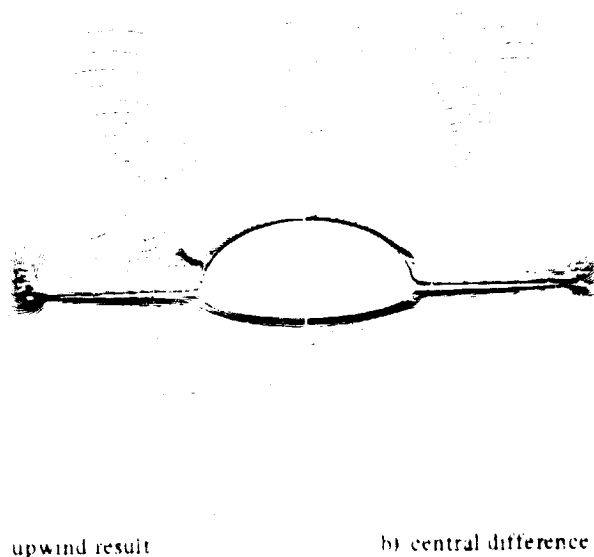
a) upwind result   b) central difference result

Fig. 10   Spanwise plots of the computed density contours over a spaceplane
(x/c = 98%): $M_\infty = 1.5$, $\alpha = 20°$

than the central difference scheme. In the present upwind scheme where the dissipation terms are constructed in the matrix form, each characteristic wave has its own minimum dissipation. On the other hand, central difference scheme where dissipation terms are constructed in the scalar form, requires amount of dissipation which is large enough for all the waves. This is the main reason that the present upwind is less dissipative and has better resolution. Thus, the use of the proper upwind scheme is recommended for vortical flow simulations at high

Reynolds number.

From the solution presented here, another important conclusion may be that it is dangerous to discuss physics of separated vortical flows based on the numerical solutions without sufficient resolution. It may be necessary to simulate the flow field with a sequence of grid cell size even with the high-order upwind schemes.

ACKNOWDGEMENT

REFERENCES

1) Newsome, R.W. and Kandil, O.A., "Vortical Flow Aerodynamics–Physical Aspects and Numerical Simulation," AIAA Paper 87-0205, 1987.

2) Rai. M.M., "Navier-Stokes Simulations of Blade-Vortex Interaction Using High-Order Accurate Upwind Schemes," AIAA Paper 87-05437, 1987.

3) Fujii, K., Gavali, S. and Holst, T.L., "Evaluation of Navier-Stokes and Euler Solutions for Leading-edge Separation Vortices," Proc. ICNMLTF, July, 1987, also as NASA TM 89458, 1987.

4) Thomas, J.L., Taylor, S.L. and Anderson, K.A., "Navier-Stokes Computations of Vortical Flows over Low Aspect Ratio Wing," AIAA Paper 87-0207, 1987.

5) Ogawa, S., Ishiguro, T. and Takakura, Y., "Numerical Simulations of Flow Field around Three-Dimensional Complex Configurations," Proc. 7th GAMM Workshop on Num. Meth. in Fluid Mech., Sept., 1987.

6) Klopfer, G.kH. and Yee, H.C., "Viscous Hypersonic Shock-On-Shock Interaction on Blunt Cowl Lips," AIAA Paper 87-0233, Jan., 1987.

7) Van Leer, B., Thomas, J.L., Roe, P.L. and Newsome, R.W., "A Comparison of Numerical Flux Formulas for the Euler and Navier-Stokes Equations," AIAA Paper 87-1104CP, June, 1987.

8) Roe, P.L., "Finite-Volume Methods for the Compressible Navier-Stokes Equations," Proc. Int. Conf. Num. Methods for Laminar and Turbulent Flows, July, 1987.

9) Vatsa, V.N., Thomas J.L. and Wedan, B.W., "Navier-Stokes Computations of Prolate Spheroids at Angle of Attack," AIAA Paper 87-2627, 1987.

10) Obayashi, S., Matsushima, K. Fujii, K. and Kuwahara, K., "Improvements in Efficiency and Reliability for Navier-Stokes Computations Using the LU-ADI Factorization Algorithm," AIAA Paper 86-338, Jan., 1986.

11) Fujii, K. and Obayashi, S., "Navier-Stokes Simulations of Transonic Flows over a Practical Wing Configuration," AIAA J., Vol. 25, No. 3, March, 1987, pp. 369-370.

12) Roe, P.L., "Characteristic-Based Schemes for the Euler Equations," Ann. Rev. Fluid Mech., 1986, pp. 337-365.

13) Fujii, K. and Obayashi, S., "Navier-Stokes Simulations of Transonic Flows over Wing-Fuselage Combination," AIAA J., Vol. 25, No. 12, Dec., 1987, pp. 1587-1596.

14) Brennenstuhl, U. and Hummel, D., "Vortex Formation over Double-Delta Wings," ICAS Paper 82-6.6.3, Proc. of 13th Congress on Int. Coun. of the Aero. Sci., Aug., 1982.

15) Fujii, K. and Schiff, L.B., "Numerical Simulation of Vortical Flows over a Strake-Delta Wing." AIAA Paper 87-1229, 1987, also to appear in the AIAA J.